Iron control of past productivity in the coastal upwelling system off the Atacama Desert, Chile

Laurent Dezileau, Osvaldo Ulloa, Dierk Hebbeln, Frank Lamy, Jean-Louis Reyss, Michel Fontugne

Iron control of past productivity in the coastal upwelling system off the Atacama Desert, Chile

Laurent Dezileau,[1,2] Osvaldo Ulloa,[1] Dierk Hebbeln,[3] Frank Lamy,[3]
Jean-Louis Reyss,[4] and Michel Fontugne[4]

Received 12 January 2004; revised 25 May 2004; accepted 25 June 2004; published 16 September 2004.

[1] Biogenic opal and organic carbon vertical rain rates in sediment cores reveal a strong cyclicity in the productivity of the upwelling system off presently arid northern Chile during the last 100,000 years. Changes in productivity are found to be in phase with the precessional cycle (~20,000 years) and with inputs of iron from the continent. During austral summer insolation maxima, increased precipitation and river runoff in the region appear to have brought high inputs of iron, mainly from the Andes, to the coastal ocean enhancing primary productivity there. We interpret our results as providing evidence for iron control of past productivity in this upwelling system and for a tight link between productivity and orbital forcing at midlatitudes. *INDEX TERMS:* 4267 Oceanography: General: Paleoceanography; 4825 Oceanography: Biological and Chemical: Geochemistry; 4860 Oceanography: Biological and Chemical: Radioactivity and radioisotopes; *KEYWORDS:* paleoproductivity, thorium-230, iron, coastal upwelling, biogenic opal, organic carbon

Citation: Dezileau, L., O. Ulloa, D. Hebbeln, F. Lamy, J.-L. Reyss, and M. Fontugne (2004), Iron control of past productivity in the coastal upwelling system off the Atacama Desert, Chile, *Paleoceanography*, *19*, PA3012, doi:10.1029/2004PA001006.

1. Introduction

[2] Since the hypothesis was established that variations of marine biological productivity might be one of the mechanisms responsible for glacial/interglacial pCO_2 changes [*Broecker*, 1982] much effort has been put into the reconstruction of paleoproductivity. Most of the studies have been performed on sediments underlying high nutrient-low chlorophyll (HNLC) regions and the high productivity areas of the world's oceans: the Southern Ocean, the equatorial upwelling regions and the eastern boundary current systems.

[3] Eastern boundary currents are systems of enhanced biological productivity that contribute a significant fraction of the global primary production and burial of organic carbon [*Brink and Cowles*, 1991; *Longhurst et al.*, 1995; *Summerhayes et al.*, 1995]. There wind-driven coastal upwelling brings subsurface waters rich in major nutrients into the photic zone where they are capable of fertilizing the otherwise nutrient-poor surface waters. Past changes in the productivity of these regions have commonly been explained in terms of changes in the intensity of upwelling-favorable winds, and therefore in the availability of macro nutrients [*Arrhenius*, 1952; *Berger et al.*, 1989; *Sarnthein et al.*, 1988]. However, recent experiments [*Hutchins and Bruland*, 1998; *Hutchins et al.*, 2002] have demonstrated that in two major coastal upwelling systems, the California and the Peru-Chile ecosystems, phytoplankton growth can also be limited by iron, a micronutrient which has additional sources to upwelling deep waters. In these regions where riverine and atmospheric inputs are negligible, and where the continental shelf is very narrow, iron limitation is a major constraint on phytoplankton growth. Despite accumulating evidence for iron limitation in these modern coastal upwelling systems, paleoceanographic studies have not yet revealed evidence for a link between past changes of iron availability and biological productivity. Here we report on biogenic opal, organic carbon and iron accumulation rates (corrected for sediment redistribution by ^{230}Th-normalization) obtained from sediment cores retrieved from the upwelling system off presently arid northern Chile and we provide evidence for iron control of past productivity in this upwelling system.

2. Study Area, Material, and Method

[4] We have analyzed variations of ocean productivity through time in the upwelling system of the eastern South Pacific, as recorded in sediments from two gravity cores (GeoB 7101-1 and GeoB 3375-1, Figure 1) retrieved at the same location from the continental slope off northern Chile (27°28′S, 71°15′W, 1956 and 1947 m water depth respectively). This perennial upwelling system is characterized by an extremely narrow shelf, only 10 to 15 km wide on average. Its surface waters present relatively high concentrations of nitrate and phosphate, low concentrations of silicate and phytoplankton pigment (Figure 1), as well as

[1]Centro de Investigación Oceanográfica, Programa Regional de Oceanografia Fisica y Clima, Departamento de Oceanografía, Universidad de Concepción, Concepción, Chile.
[2]Now at Laboratoire de Dynamique de la Lithosphère, Université de Montpellier 2, Montpellier, France.
[3]Fachbereich Geowissenschaften, Universität Bremen, Bremen, Germany.
[4]Laboratoire des Sciences du Climat et de l'Environnement, CNRS/Commissariat à l'Energie Atomique, Gif-sur-Yvette, France.

0883-8305/04/2004PA001006

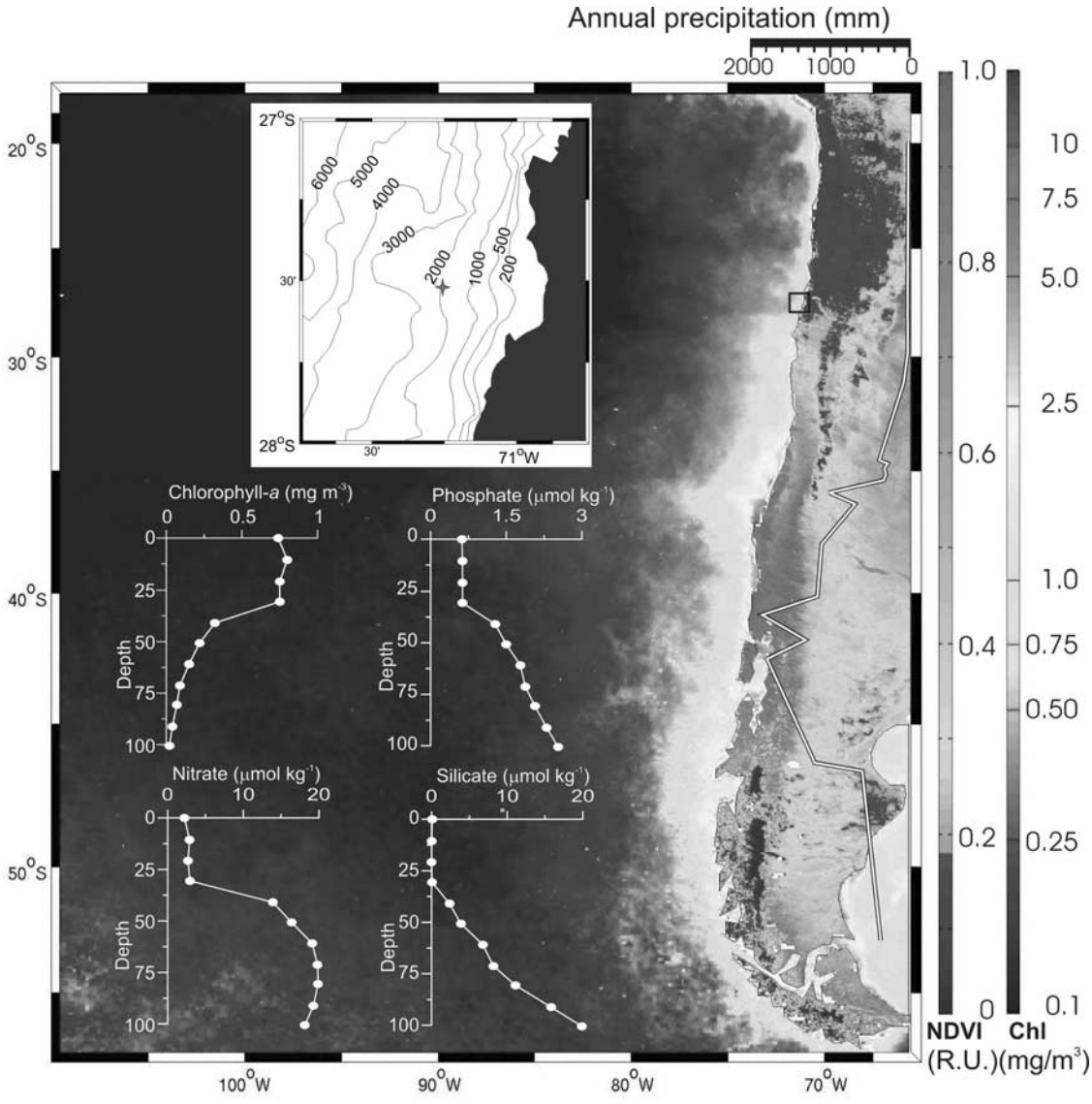

Figure 1. Composite of annual average of phytoplankton pigment concentration (Chl) of the eastern South Pacific and annual maximum normalized difference vegetation index (NDVI) of the central and southern Andean region (both for year 2000). These data were derived from the SeaWiFS sensor (SeaWiFS Project) Distributed Active Archive Center. Top left inset: map of the study area with location of the two cores GeoB 3375-1 and GeoB 7101-1 (27°28′S, 71°15′W). Bottom left inset: chlorophyll and nutrient profiles of the upper 100 m depth at station GeoB 3377-1 (27°28′S; 71°31.5′W). Right inset: average of annual continental rainfall data in Chile (http://www.meteochile.cl). See color version of this figure at back of this issue.

a relatively low primary production [*Daneri et al.*, 2000], all characteristics of iron limited HNLC systems [*Hutchins and Bruland*, 1998; *Hutchins et al.*, 2002]. The modern climate of the continental region adjacent to the sampling position (the southern limit of the Atacama Desert) is hyperarid (Figure 1).

[5] Core GeoB7101-1 was sampled at 10 cm intervals using 10-ml syringes. Two samples series were taken. The first was designated for uranium, thorium (Table 1) and rare Earth elements analyses and the second for carbonate concentration measurements. The dry bulk density of the sediments was measured by weighting a fixed sample volume before and after freeze-drying (Table 1). Uranium and thorium concentrations were measured by α spectrometry following separation on anion exchange columns and deposition onto aluminum foil. The analytical uncertainty of the ^{230}Th concentration data from counting statistics was 5%. Samples were only occasionally run in duplicate and uncertainties of the reproductibilities were less than or equal to those from counting statistics. The analytical uncertainty of ^{238}U concentration measurements from counting statistics was 6%. The carbonate content (% CaCO3) has been

Table 1. Results Obtained on Marine Sediment Samples for Cores GeoB 3375-1 and GeoB 7101-1[a]

GeoB 7101-1 Depth, cm	Age, kyr	DBD, g/cm3	238U, dpm/g	232Th, dpm/g	230Th, dpm/g	230Thex, dpm/g	230Thex°, dpm/g	238U auth, dpm/g	Geob 3375 Depth, cm	Age, kyr	Org C, %	Opal, %	Detrital Material, %	Iron, ppm
3	9.7	0.87	1.51 ± 0.11	1.39 ± 0.11	3.94 ± 0.24	2.86 ± 0.25	3.13 ± 0.28	0.47 ± 0.13	3	9.7	0.43 ± 0.02	0.70 ± 0.14	81.94	26047
8	10.3	1.07	3.08 ± 0.18	1.41 ± 0.10	4.06 ± 0.24	2.82 ± 0.25	3.10 ± 0.28	2.02 ± 0.19	8	10.3	0.41 ± 0.02	0.60 ± 0.12	77.65	25997
18	12.2	1.05	5.03 ± 0.19	1.42 ± 0.10	4.08 ± 0.21	2.59 ± 0.22	2.90 ± 0.25	3.97 ± 0.20	18	12.2	0.52 ± 0.03	0.40 ± 0.08	74.07	24589
23	13.2	0.96	5.14 ± 0.22	1.47 ± 0.19	3.94 ± 0.37	2.38 ± 0.38	2.68 ± 0.43	4.04 ± 0.25	23	13.2	0.65 ± 0.03	0.30 ± 0.06	75.19	26123
33	15.2	1.00	3.88 ± 0.19	1.57 ± 0.10	4.02 ± 0.18	2.49 ± 0.19	2.86 ± 0.22	2.70 ± 0.20	33	15.2	0.53 ± 0.03	0.60 ± 0.12	80.90	27356
48	16.7	1.09	2.60 ± 0.55	1.95 ± 0.17	3.25 ± 0.25	1.62 ± 0.28	1.89 ± 0.33	1.13 ± 0.56	48	16.7	0.52 ± 0.03	0.75 ± 0.15	85.91	28353
63	18.1	1.18	2.15 ± 0.15	1.79 ± 0.15	2.90 ± 0.20	1.44 ± 0.22	1.70 ± 0.26	0.81 ± 0.17	63	18.1	0.48 ± 0.02	0.80 ± 0.16	87.73	28177
78	19.5	1.12	2.23 ± 0.12	2.03 ± 0.08	3.20 ± 0.12	1.56 ± 0.13	1.87 ± 0.15	0.71 ± 0.13	78	19.5	0.46 ± 0.02	0.75 ± 0.15	86.36	32282
93	21.1	1.14	2.14 ± 0.16	1.85 ± 0.13	2.67 ± 0.17	1.16 ± 0.19	1.40 ± 0.23	0.76 ± 0.18	93	21.1	0.48 ± 0.02	0.70 ± 0.14	87.64	34005
103	22.2	1.17	1.95 ± 0.08	1.72 ± 0.04	2.67 ± 0.06	1.26 ± 0.07	1.55 ± 0.09	0.66 ± 0.08	103	22.2	0.45 ± 0.02	0.80 ± 0.16	87.20	32400
128	25.2	1.11	2.69 ± 0.33	1.71 ± 0.12	3.01 ± 0.19	1.44 ± 0.22	1.81 ± 0.27	1.40 ± 0.34	128	25.2	0.75 ± 0.04	0.95 ± 0.19	85.00	32245
153	28.7	1.12	2.48 ± 0.11	1.57 ± 0.07	3.94 ± 0.15	2.46 ± 0.16	3.20 ± 0.20	1.30 ± 0.12	153	28.7	0.69 ± 0.03	1.10 ± 0.22	85.07	30279
163	30.0	1.16	2.93 ± 0.30	1.43 ± 0.05	3.58 ± 0.10	2.06 ± 0.12	2.71 ± 0.16	1.86 ± 0.30	163	30.0	0.80 ± 0.04	0.70 ± 0.14	81.09	25247
173	34.6	1.23	3.30 ± 0.07	1.57 ± 0.08	3.71 ± 0.15	1.95 ± 0.16	2.69 ± 0.22	2.13 ± 0.08	173	34.6	0.59 ± 0.03	0.60 ± 0.12	81.37	25740
178	36.9	1.23	3.65 ± 0.11	1.42 ± 0.06	3.63 ± 0.13	1.82 ± 0.14	2.56 ± 0.19	2.58 ± 0.11	178	36.9	0.41 ± 0.02	0.65 ± 0.13	79.41	24572
193	40.3	1.18	3.36 ± 0.10	1.36 ± 0.08	3.18 ± 0.14	1.43 ± 0.16	2.07 ± 0.22	2.35 ± 0.11	193	40.3	0.58 ± 0.03	0.60 ± 0.12	80.35	29429
208	42.7	1.17	2.32 ± 0.14	1.51 ± 0.09	2.81 ± 0.15	1.29 ± 0.17	1.91 ± 0.25	1.19 ± 0.15	208	42.7	0.58 ± 0.03	0.80 ± 0.16	81.47	28684
223	47.2	1.18	2.73 ± 0.15	1.74 ± 0.14	2.85 ± 0.20	1.05 ± 0.22	1.62 ± 0.34	1.42 ± 0.17	223	47.2	0.69 ± 0.03	0.70 ± 0.14	83.40	31029
238	51.0	1.25	2.38 ± 0.09	1.94 ± 0.07	3.02 ± 0.10	1.21 ± 0.12	1.94 ± 0.19	0.93 ± 0.10	238	51.0	0.53 ± 0.03	0.80 ± 0.16	83.23	30481
253	54.8	1.18	2.63 ± 0.14	2.00 ± 0.13	3.69 ± 0.21	1.74 ± 0.23	2.88 ± 0.38	1.14 ± 0.16	253	54.8	0.65 ± 0.03	0.70 ± 0.14	79.53	26514
263	57.4	1.24	3.22 ± 0.16	1.62 ± 0.13	3.47 ± 0.23	1.43 ± 0.25	2.43 ± 0.43	2.00 ± 0.18	263	57.4	0.69 ± 0.03	0.50 ± 0.10	81.68	26040
273	59.9	1.29	2.38 ± 0.17	1.44 ± 0.09	3.37 ± 0.16	1.74 ± 0.19	3.02 ± 0.33	1.30 ± 0.18	273	59.9	0.60 ± 0.03	0.50 ± 0.10	83.15	26148
293	65.0	1.17	2.98 ± 0.07	1.39 ± 0.10	3.03 ± 0.17	1.11 ± 0.18	2.02 ± 0.33	1.94 ± 0.09	293	65.0	0.80 ± 0.04	0.70 ± 0.14	81.88	28981
313	69.8	1.24	2.88 ± 0.08	1.74 ± 0.06	3.03 ± 0.09	0.98 ± 0.10	1.87 ± 0.20	1.57 ± 0.09	313	70.5	0.58 ± 0.03	0.80 ± 0.16	83.86	32879
333	73.9	1.22	2.66 ± 0.20	1.88 ± 0.07	2.86 ± 0.10	0.83 ± 0.15	1.65 ± 0.30	1.24 ± 0.21	323	73.2	0.54 ± 0.03	0.70 ± 0.14	86.39	33223
343	75.9	1.24	2.38 ± 0.09	1.95 ± 0.07	2.97 ± 0.10	1.04 ± 0.12	2.10 ± 0.24	0.91 ± 0.10	333	75.9	0.63 ± 0.03	1.00 ± 0.20	87.84	33039
353	78.1	1.13	2.62 ± 0.12	1.76 ± 0.09	3.24 ± 0.14	1.26 ± 0.16	2.58 ± 0.33	1.31 ± 0.13	343	78.6	0.56 ± 0.03	1.40 ± 0.28	84.59	30914
363	80.3	1.19	2.95 ± 0.15	1.54 ± 0.06	3.17 ± 0.10	1.07 ± 0.13	2.25 ± 0.28	1.79 ± 0.15	353	81.4	0.67 ± 0.03	1.10 ± 0.22	80.10	28266
373	82.5	1.17	3.52 ± 0.13	1.33 ± 0.08	3.54 ± 0.17	1.20 ± 0.19	2.57 ± 0.40	2.53 ± 0.14	363	84.1	0.63 ± 0.03	1.00 ± 0.20	78.61	25225
383	89.5	1.11	3.85 ± 0.20	1.50 ± 0.10	3.57 ± 0.17	0.91 ± 0.22	2.08 ± 0.49	2.72 ± 0.20	383	89.5	0.50 ± 0.03	0.80 ± 0.16	78.03	28111
403	95.0	1.21	2.75 ± 0.13	1.77 ± 0.08	2.90 ± 0.11	0.74 ± 0.14	1.78 ± 0.34	1.42 ± 0.14	403	95.0	0.39 ± 0.02	1.00 ± 0.20	87.92	33803
409	96.4	1.25	2.45 ± 0.10	1.83 ± 0.11	2.89 ± 0.16	0.88 ± 0.18	2.13 ± 0.45	1.08 ± 0.12	408	96.4	0.50 ± 0.02	1.00 ± 0.20	87.21	31965

[a]The dry bulk density (DBD) of the sediments was measured by weighting a fixed sample volume before and after freeze-drying. Uranium and thorium concentrations were measured by α spectrometry. $^{230}Th^{\circ}_{ex}$ refers to excess ^{230}Th activity in sediments decay-corrected to the time of deposition. ^{238}U auth refers to excess U above detrital background levels. The biogenic opal content was measured applying the method of *Müller and Schneider* [1993]. Organic carbon analyses were conducted with an Hereaus CHN-O-rapid. The detrital fraction of the sediment was estimated from bulk sediment weight minus biogenic components. The iron data have been previously published in the work of *Lamy et al.* [2000].

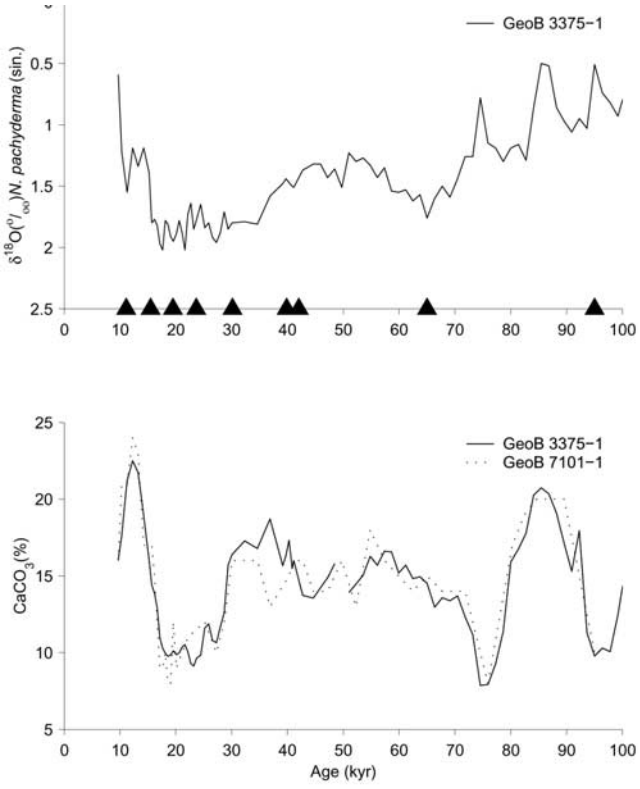

Figure 2. Age model for sediment core GeoB 3375-1 and GeoB 7101-1. (top) $\partial^{18}O$(‰) curve of the planktic foraminifera *N. pachyderma* (sin.) and age control points (indicated by triangle) include seven AMS ^{14}C dates and two graphical correlation points of the $\partial^{18}O$ records to a standard $\partial^{18}O$ curve. (bottom) Carbonate content for the cores GeoB 3375-1 and GeoB 7101-1. We obtained the chronology for the core GeoB 7101-1 by graphically correlating its carbonate content variations with those of core GeoB 3375-1. The used standard methods for $\partial^{18}O$ analysis, AMS dating, and carbonate content determinations are described elsewhere in detail [*Lamy et al.*, 1998].

determined with a calcimeter by the CO_2 volumetric method. The precision is estimated to be about 2%. Analyses of La and Yb were carried out by Epithermal Neutron Activation Analysis (ENAA) at the Pierre Sue Laboratory (Saclay, France). Two USGS standards, Mag 1 and A1, were used. Sediment samples and standards were enclosed in plastic bags. After irradiation, sediment samples and standards were measured with an HP Ge detector (FWMH 1.7 keV at 1332 keV; relative efficiency: 20%) at the Laboratoire des Sciences du Climat et de l'Environnement. The precision is estimated to be about 5%.

[6] The biogenic opal content was measured on core GeoB 3375-1 (D. Hebbeln, unpublished results, 2001) applying the method of *Müller and Schneider* [1993] and the values obtained were between 0.3 and 1.4%. For samples with low opal contents (<1 wt %) the uncertainty of the method used is of 20% and for samples with very low opal contents (<0.5 wt %) the uncertainty is about 60% (Table 1). Organic carbon analyses of core GeoB 3375-1 were conducted with an elemental analyzer (Hereaus CHN-O-Rapid) on HCl-treated samples (Table 1). The detrital fraction of the sediment was estimated from the bulk sediment weight minus the biogenic components (opal, carbonate, organic matter) with detrital fraction = 1 − (opal fraction + carbonate fraction + 3 × organic carbon fraction) [*Dezileau et al.*, 2000]. The iron (Table 1) and aluminum data used in this study were previously reported in the work of *Lamy et al.* [2000].

3. Chronology

[7] The age model for core GeoB 3375-1 is based on both AMS ^{14}C ages and $\partial^{18}O$ records of *N. pachyderma* (sin.) [*Lamy et al.*, 1998] resulting in an age of ~117.000 cal years BP at the base of the core (Figure 2). The chronology for core GeoB 7101-1 has been obtained by correlating graphically its carbonate content variations with those of core GeoB 3375-1, using the Analyseries Software [*Paillard et al.*, 1996] (Figure 2). On this basis, core GeoB 7101-1 covers the last 100,000 cal years BP, with an average sedimentation rate of 5 cm/1000 years. These twin cores come from almost exactly the same location and have the same age at each depth up to 300 cm. This suggests that if these cores have been affected by sediment redistributions, these effects were of same intensities in the past.

4. Vertical Fluxes Calculations

[8] Although past changes in ocean productivity can be assessed, in principle, from the record of biogenic detritus buried in the seabed, their interpretation is often hampered by sediment redistribution processes (focusing or winnowing) and variable dissolution. We have calculated preserved vertical rain rates to the seafloor by normalizing biogenic component fluxes to the corresponding excess ^{230}Th activity in the sediments, a method that corrects for sediment focusing and winnowing [*Bacon*, 1984; *Suman and Bacon*, 1989; *François et al.*, 1990, 2004].

[9] Thorium-230 normalized flux calculations are based on the assumption that the flux of ^{230}Th to the seafloor is constant and equal to the rate of production [*Bacon*, 1984; *Suman and Bacon*, 1989; *François et al.*, 1990, 2004]. Excess ^{230}Th activity in settling particulates is then inversely related to total mass flux, and excess ^{230}Th activities (to see how is obtained the age-corrected excess ^{230}Th activity see Appendix A) in the sediment can be used as reference against which the flux of other sedimentary components can be estimated:

$$F_i = \frac{\beta . Z . f_i}{^{230}Th^{\circ}_{ex}}, \quad (1)$$

where F_i is the normalized rain rate of the sedimentary component i; β is the constant production rate of ^{230}Th in the water column (2.63×10^{-5} dpm cm^{-3} kyr^{-1}); Z is the water depth (cm); f_i is the percentage of the sedimentary component i; and $^{230}Th^{\circ}_{ex}$ is the activity of decay- and ingrowth-corrected excess ^{230}Th in sediment.

[10] Arguments for the validity of this approach have been examined elsewhere [*Henderson et al.*, 1999; *Yu et al.*,

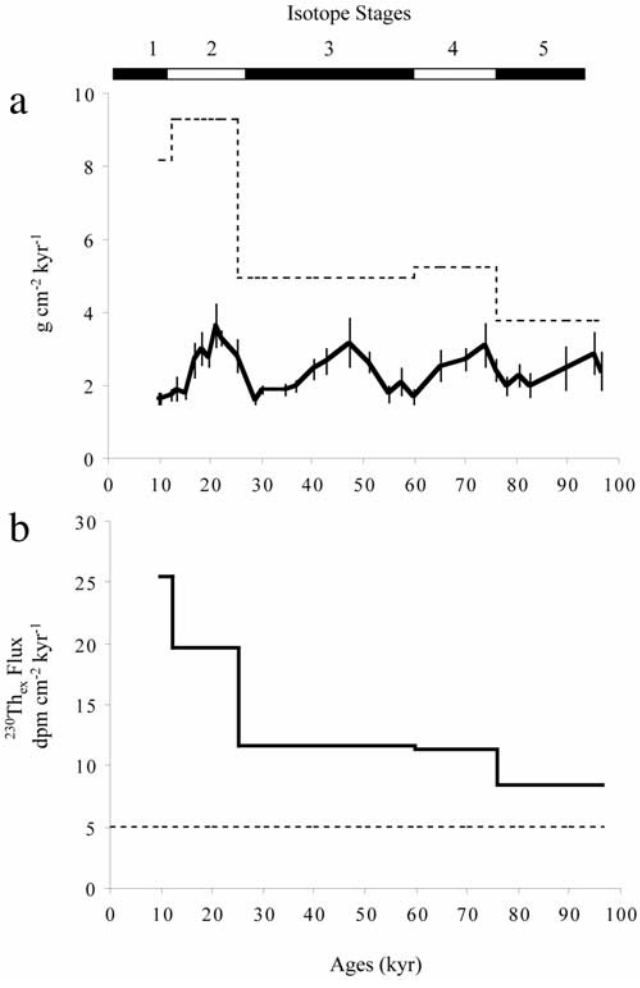

Figure 3. (a) Comparison between sediment accumulation rate and vertical particle rain rate for core GeoB 7101-1. Sediment accumulation rates (dotted line) for the last 100,000 years based on mass accumulated between oxygen isotope stage boundaries. Vertical particle rain rate (solid line) is based on point-by-point normalization to $^{230}Th^{\circ}_{ex}$ applying the constant flux model. (b) $^{230}Th^{\circ}_{ex}$ flux in dpm cm^{-2} kyr^{-1} versus age for each $\partial^{18}O$ isotope stages. The stippled line marks the expected flux of 5.14 dpm cm^{-2} kyr^{-1} at this location.

2001]. This approach was successfully applied where lateral re-sedimentation is important [*Suman and Bacon*, 1989; *François et al.*, 1993, 1997; *Kumar et al.*, 1995; *Anderson et al.*, 1998, 2002; *Frank et al.*, 1995, 2000; *Dezileau et al.*, 2000, 2003; *Chase et al.*, 2003].

5. Results

5.1. Vertical Sediment Rain Rates Compared With Sediment Accumulations Rates

[11] When comparing the sediment accumulation rates to the vertical particle rain rates calculated by the $^{230}Th^{\circ}_{ex}$ method [see *Suman and Bacon*, 1989, equation (A2); *François et al.*, 1993, 1997, 2004], we note striking differences between the two records (Figure 3a). The accumulation rates on the seafloor during the Holocene and marine oxygen isotope stage (MIS) 2, were 5.0 and 3.7 times higher, respectively, than the vertical rain rates. During MIS 5 to 3, the accumulation rates were only 2.1 times higher than the vertical rain rates.

[12] These differences are probably due to an increase of focusing during these periods, however, it may also be possible that the estimation of the vertical rain rates by the $^{230}Th^{\circ}_{ex}$ method is biased because the assumption underlying the constant flux model of ^{230}Th is not valid. Having shown that these problems are negligible for our cores (see Appendix B), we conclude that the focusing factor is a reliable quantitative proxy to correct for lateral sediment redistribution in this region.

[13] The difference between the sediment accumulation rate and the vertical sediment rain rate is pronounced and has mainly been caused by an increase of focusing intensity, in particular during the Holocene and LGM. The reconstruction of paleoproductivity would be quite different if only the accumulation rates had been used without the $^{230}Th^{\circ}_{ex}$-normalization. The nonnormalized accumulation rates do not show any climate related variation. With the $^{230}Th^{\circ}_{ex}$-normalization, the vertical sediment rain rates reveal a strong cyclicity which is dominated by precessional cycles. This illustrates the importance of the $^{230}Th^{\circ}_{ex}$-normalization method for reconstructions of past particle fluxes.

5.2. Records of Terrigenous Composition off the Norte Chico (27.5°S)

[14] The sediments consist mainly of terrigenous material with contents between 75 and 88 wt % (Figure 4a). The iron content (Figure 4b) varies between 24000 and 34000 ppm [*Lamy et al.*, 2000]. *Lamy et al.* [2000] used the Fe/Al ratio in gravity core GeoB 3375-1 (located in the same area) to estimate past changes in terrigenous sediment provenance (Figure 4c). In their study, they interpreted changes in the Fe/Al ratio of the bulk sediment as a terrigenous signal, which is determined by relative contributions of two source areas, i.e., the Andes and the Coastal Range. Observed variations could also have been produced by changes in the proportions of two components in the sediment, a detrital component with a low and constant Fe/Al ratio and a variable amount of an authigenic phase (Fe oxide, pyrite, apatite, etc.) with a high Fe/Al ratio. However, we have also analyzed rare Earth elements (REE) by neutron activation in the same core. In particular we have used the La/Yb to determine the origin of the detrital particles (Figure 4c). The advantage of the La/Yb ratio over the Fe/Al is that the lithogenic signal of the bulk sediment is not altered by changes in redox conditions. The Coastal Range consists primarily of Mesozoic calc-alkaline plutonic rocks (granites) and is characterized by La/Yb ratios between 8 and 9.2 [*Pichowiak*, 1994]. The Andes consist primarily of Plio-Quaternary volcanism, including andesitic and rhyolitic rocks characterized by La/Yb ratios between 10.6 and 18 [*Kay et al.*, 1991]. The La/Yb ratios in our core are below 9.5 during periods of low iron contents, indicating a dominating contribution of terrigenous particles from the Coastal Range source (Figure 4c). These ratios increase

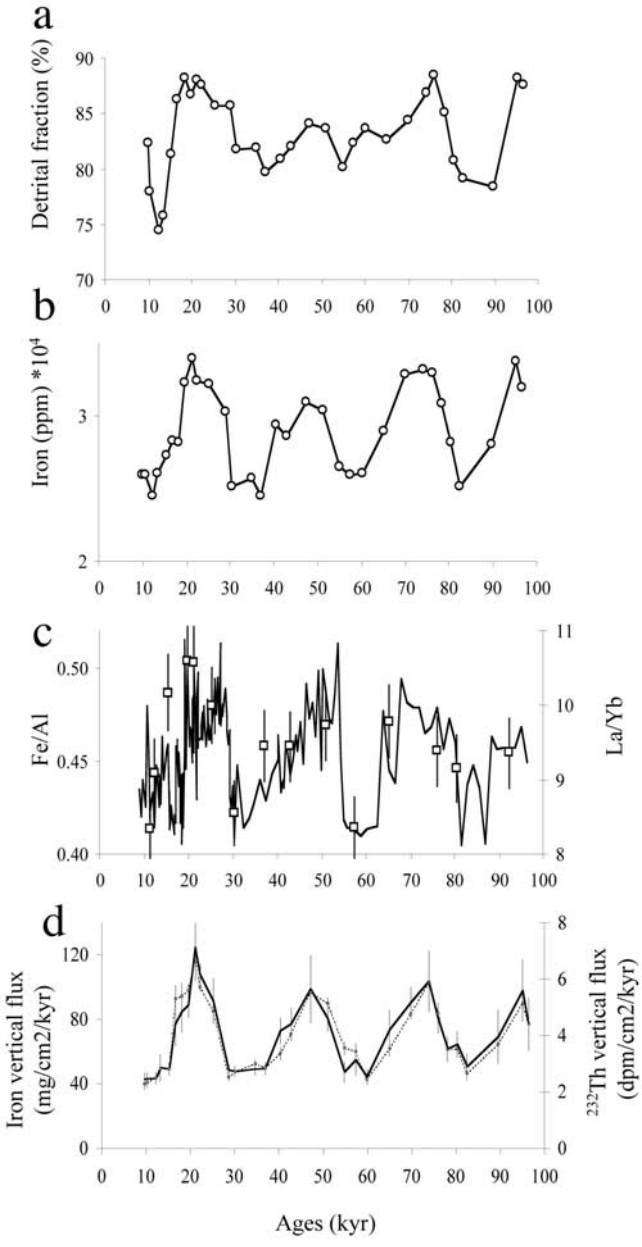

Figure 4. Comparison of geochemical data for the last 100,000 years derived from deep-sea sediment cores GeoB 3375-1 and GeoB 7101-1. (a) The detrital fraction (%). (b) Iron content in ppm($\times 10^4$). (c) The Fe/Al (line) and La/Yb (square) ratio. (d) Comparison between iron (solid line) and ^{232}Th vertical fluxes (dotted line).

during periods of high iron contents, indicating a likely relative increase in the volcanic contribution, i.e., from the Andes. The La/Yb ratios thus support the conclusions obtained from Fe/Al ratios. We then assume that the presence of authigenic iron is negligible in our core and that the Fe/Al ratio can be used to reconstruct past changes of the lithogenic material in this core. The terrigenous origin of iron is also confirmed by an excellent correlation between iron and ^{232}Th vertical rain rates (^{232}Th is considered to be exclusively present in detrital minerals; $r^2 = 0,91$, Figure 4d).

5.3. Records of Biogenic Constituents off the Norte Chico (27.5°S)

5.3.1. Organic Carbon

[15] Varying organic carbon fluxes in hemipelagic sediments below eastern boundary current systems are primarily controlled by surface water productivity and thus can be used as a direct proxy for paleoproductivity in such environments [*Lyle et al.*, 1988; *Sarnthein et al.*, 1988; *Berger et al.*, 1989; *Pedersen and Calvert*, 1990; *Schneider et al.*, 1997]. However, in a region marked by a strong terrigenous input, the organic carbon content of the marine sediments can be increased by a certain portion of terrigenous organic matter, which might bias paleoproductivity estimates based on organic carbon accumulation. This problem can be addressed by using δ^{13}Corg data, which are often used to detect contributions of terrestrial organic matter to marine sediment. Terrestrial organic matter usually has δ^{13}Corg values of -28 to -26‰ [*Emerson and Hedges*, 1988], while marine plankton has typical δ^{13}Corg values of -22 to -19‰ for water temperatures between 13 and 18°C [*Fontugne and Duplessy*, 1981]. The δ^{13}Corg data in the surface sediments vary between -21.97 and -20.48. Thus, although our gravity core has been collected very close to the coast, the δ^{13}Corg data do not give any hint for a substantial input of terrigenous organic matter. For all our samples δ^{13}Corg lies well inside the typical ranges for marine organic matter, which seems to clearly dominate the total organic carbon content. Keeping in mind that on average 80% of the sediment material is of terrigenous origin, the terrestrial organic carbon input seems to have been rather low. On the other hand, a significant contribution from C4 plants, characterized by high δ^{13}C values, can be discarded due to the very low vegetation biomass of this desert or steppic environment. Furthermore, *Quay et al.* [1992] showed that the contribution of C4 plants to open ocean sediments is low, because of their preferential oxidation in rivers. *Mariotti et al.* [1991] showed that the organic carbon isotopic composition of suspended material in the Congo river presents typical C3 plant values, in spite of the occurrence of large savanna areas covered by C4 plants in the hydrographic basin. Similar results were found in sediments off India by *Bentaleb et al.* [1997].

5.3.2. Opal and Organic Carbon Vertical Fluxes

[16] The calculated vertical sediment rain rates were combined with the sedimentological analyses in order to assess component vertical rain rates (Table 2). Organic carbon vertical rain rates varied by more than a factor of 3, and the opal vertical rain rates varied by a factor of 6 (Figures 5a and 5b). These variations were in phase during the last 100,000 years. Variation in sedimentation rates can affect opal and organic matter preservation. Thus it could be argued that the ups and downs in opal and organic carbon fluxes are mainly driven by preservation effects. However, we do not find any correlation between organic matter content and sediment accumulation/vertical particle rain rate, nor between opal content and sediment accumulation/vertical particle rain rate. Thus we do not have any

Table 2. Vertical Flux Refers to ^{230}Th Normalized Total Mass Accumulation Rate, Organic Carbon (Opal and Iron) Vertical Flux Refers to ^{230}Th Normalized Organic Carbon (Opal and Iron) Accumulation Rate[a]

Age, Kyr	230Thex°, dpm/g	Vertical Flux (230Th Method), g/cm2/kyr	Org C Vertical Flux (230Th Method), mg/cm2/kyr	Opal Vertical Flux (230Th Method), mg/cm2/kyr	Iron Vertical Flux (230Th Method), mg/cm2/kyr	Opal/CaCO3	Authigenic Uranium Accumulation Rate, dpm/cm2/kyr
9.7	3.13 ± 0.28	1.64 ± 0.14	7.09 ± 0.62	11.51 ± 1.01	42.82 ± 3.77	0.044 ± 0.009	3.48
10.3	3.10 ± 0.28	1.66 ± 0.15	6.75 ± 0.60	9.97 ± 0.89	43.20 ± 3.85	0.029 ± 0.006	10.96
12.2	2.90 ± 0.25	1.77 ± 0.15	9.13 ± 0.78	7.09 ± 0.61	43.58 ± 3.74	0.017 ± 0.003	21.14
13.2	2.68 ± 0.43	1.92 ± 0.31	12.42 ± 2.01	5.75 ± 0.93	50.07 ± 8.09	0.013 ± 0.003	19.65
15.2	2.86 ± 0.22	1.80 ± 0.14	9.46 ± 0.73	10.79 ± 0.84	49.20 ± 3.82	0.035 ± 0.007	28.01
16.7	1.89 ± 0.33	2.72 ± 0.47	14.02 ± 2.42	20.41 ± 3.52	77.17 ± 13.31	0.064 ± 0.013	12.83
18.1	1.70 ± 0.26	3.02 ± 0.46	14.54 ± 2.21	24.19 ± 3.67	85.20 ± 12.94	0.080 ± 0.016	9.91
19.5	1.87 ± 0.15	2.76 ± 0.23	12.69 ± 1.04	20.69 ± 1.69	89.04 ± 7.26	0.065 ± 0.013	7.64
21.1	1.40 ± 0.23	3.66 ± 0.60	17.72 ± 2.90	25.63 ± 4.19	124.53 ± 20.36	0.069 ± 0.014	8.26
22.2	1.55 ± 0.09	3.33 ± 0.19	14.94 ± 0.84	26.63 ± 1.49	107.84 ± 6.04	0.075 ± 0.015	6.39
25.2	1.81 ± 0.27	2.84 ± 0.43	21.31 ± 3.21	26.99 ± 4.07	91.60 ± 13.81	0.081 ± 0.016	11.15
28.7	3.20 ± 0.20	1.61 ± 0.10	11.11 ± 0.71	17.69 ± 1.13	48.70 ± 3.10	0.094 ± 0.019	10.53
30.0	2.71 ± 0.16	1.90 ± 0.11	15.11 ± 0.91	13.28 ± 0.80	47.91 ± 2.89	0.044 ± 0.009	4.74
34.6	2.69 ± 0.22	1.92 ± 0.15	11.23 ± 0.91	11.50 ± 0.93	49.31 ± 3.98	0.037 ± 0.007	5.74
36.9	2.56 ± 0.19	2.01 ± 0.15	8.23 ± 0.62	13.08 ± 0.98	49.44 ± 3.70	0.040 ± 0.008	13.98
40.3	2.07 ± 0.22	2.48 ± 0.27	14.33 ± 1.55	14.88 ± 1.61	72.96 ± 7.91	0.035 ± 0.007	17.02
42.7	1.91 ± 0.25	2.69 ± 0.35	15.62 ± 2.01	21.50 ± 2.77	77.10 ± 9.93	0.050 ± 0.010	4.68
47.2	1.62 ± 0.34	3.18 ± 0.67	22.10 ± 4.64	22.29 ± 4.68	98.80 ± 20.73	0.051 ± 0.010	6.58
51.0	1.94 ± 0.19	2.65 ± 0.25	14.07 ± 1.34	21.20 ± 2.02	80.79 ± 7.70	0.056 ± 0.011	4.55
54.8	2.88 ± 0.38	1.79 ± 0.24	11.61 ± 1.54	12.50 ± 1.66	47.37 ± 6.30	0.039 ± 0.008	5.27
57.4	2.43 ± 0.43	2.12 ± 0.37	14.67 ± 2.59	10.58 ± 1.87	55.11 ± 9.72	0.032 ± 0.006	9.76
59.9	3.02 ± 0.33	1.70 ± 0.18	10.28 ± 1.11	8.51 ± 0.92	44.50 ± 4.80	0.034 ± 0.007	6.59
65.0	2.02 ± 0.33	2.55 ± 0.41	20.36 ± 3.30	17.84 ± 2.89	73.85 ± 11.98	0.047 ± 0.009	9.50
69.8	1.87 ± 0.20	2.75 ± 0.29	15.89 ± 1.66	21.99 ± 2.30	90.37 ± 9.45	0.059 ± 0.012	9.55
73.9	1.65 ± 0.30	3.12 ± 0.56	16.78 ± 3.03	21.84 ± 3.94	103.64 ± 18.72	0.062 ± 0.012	7.42
75.9	2.10 ± 0.24	2.45 ± 0.28	15.53 ± 1.80	24.50 ± 2.84	80.94 ± 9.39	0.108 ± 0.022	5.18
78.1	2.58 ± 0.33	1.99 ± 0.25	11.09 ± 1.40	27.93 ± 3.53	61.66 ± 7.79	0.113 ± 0.023	6.76
80.3	2.25 ± 0.28	2.28 ± 0.29	15.31 ± 1.92	25.13 ± 3.15	64.57 ± 8.10	0.066 ± 0.013	9.78
82.5	2.57 ± 0.40	2.00 ± 0.32	12.63 ± 1.99	20.04 ± 3.15	50.56 ± 7.95	0.054 ± 0.011	4.17
89.5	2.08 ± 0.49	2.47 ± 0.58	12.44 ± 2.93	19.74 ± 4.65	69.37 ± 16.34	0.041 ± 0.008	11.08
95.0	1.78 ± 0.34	2.90 ± 0.56	11.18 ± 2.17	28.97 ± 5.61	97.93 ± 18.98	0.101 ± 0.020	7.37
96.4	2.13 ± 0.45	2.41 ± 0.51	11.97 ± 2.52	24.13 ± 5.08	77.13 ± 16.24	0.097 ± 0.019	5.74

[a]The authigenic uranium accumulation rate is estimated by multiplying the total mass accumulation rate (g cm^{-2} kyr^{-1}) with the authigenic uranium concentration (dpm g^{-1}).

evidence that the signal we observe is due to changes in preservation.

5.3.3. Opal/CaCO3 Ratio

[17] We have used the opal/CaCO3 ratio as another index of productivity (Figure 5c). This ratio gives an idea about the siliceous/carbonate productivity, taking into account that when the productivity increases in a region this ratio generally increases. However, there are some uncertainties, which can induce false conclusions when evaluating paleoproductivity from the opal/CaCO3 ratio. Both opal and carbonate may be variably dissolved and the opal/CaCO3 ratio can be controlled by dissolution. Opal and carbonate respond differently to dissolution, as carbonate is dissolved under more acidic conditions, while opal gets dissolved under basic conditions. Thus dissolution problems can be considered negligible only if the Opal/CaCO3 record closely parallels the other paleoproductivity proxies. Here, there is a good correlation between the Opal/CaCO3 record and the organic carbon and opal vertical flux. Therefore we do not have any evidence that the opal/CaCO3 ratio in our core has been controlled by dissolution. Moreover, M. Mohtadi (University of Bremen, Germany) has counted and analyzed planktonic foraminifera assemblages in the core GeoB 3375-1 in order to know if variable dissolution of CaCO3 occurred (X. Mohtadi et al., manuscript in preparation, 2004). Mohtadi finds that the preservation of the planktonic forams is generally good to very good.

[18] To sum up, we do not want to argue that preservation has had no effect on our data, but the similar pattern for all the paleoproductivity indicators we studied, brings us to the conclusion that we really see a paleoproductivity signal in the data.

5.4. Authigenic Uranium: Proxy for Export Productivity?

[19] In oxic pore water, U is present as a soluble carbonate complex. When conditions become sufficiently reducing to initiate sulphate reduction, U is reduced to an insoluble form and precipitates. The U added to the sediment by this process (referred to as authigenic U) accumulates at a rate that depends on the level of oxygen in bottom water and on the flux of organic carbon. *Kumar et al.* [1995] showed a positive relationship between organic carbon flux (export productivity) and the accumulation rate of authigenic uranium and, assuming that a similar relationship existed in the past, proposed that down-core records of authigenic U flux could be used to constrain past changes in the flux of carbon

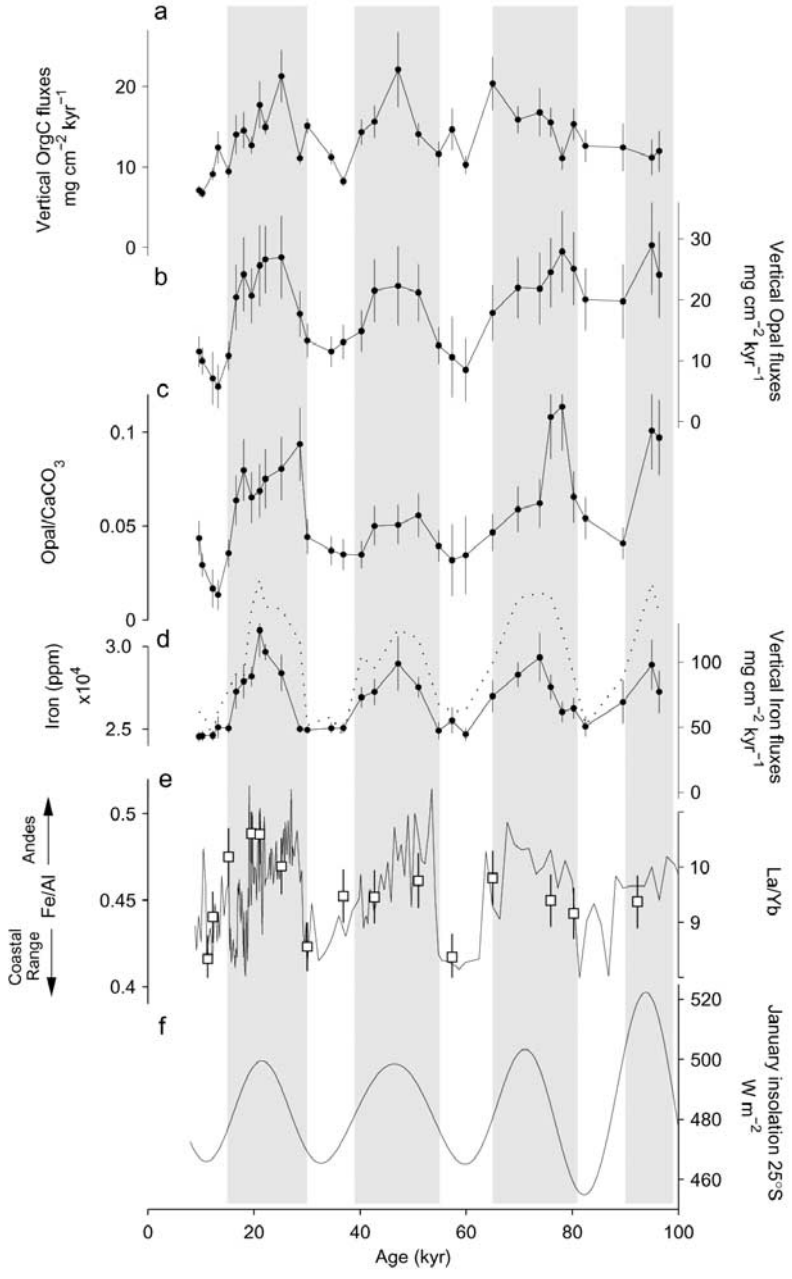

Figure 5. Comparison of geochemical data for the last 100,000 years derived from deep-sea sediment cores GeoB 3375-1 and GeoB 7101-1. (a) Organic carbon and (b) biogenic opal vertical rain rates based on point-by-point normalization to $^{230}Th^{\circ}_{ex}$. (c) Biogenic opal/carbonate ratio is also a proxy for productivity. (d) Iron content (dotted line) and iron vertical rain rates (line) based on point-by-point normalization to $^{230}Th^{\circ}_{ex}$. Terrigenous particle origin can be determined by using the Fe/Al ratio. The Fe/Al (line) (and La/Yb square) ratio of basaltic-andesitic rocks as found in the Andes is characterized by a value above 0.45 (9.5) and the Fe/Al (La/Yb) ratio of acidic-plutonic rocks, as found in the coastal range is characterized by a ratio under 0.45 (9.5). Measured Fe/Al ratios clearly show a higher contribution of terrigenous particles from the Andes during (e) precessional (summer insolation) maxima.

to the deep sea. Thus we have decided to estimate authigenic U flux in the core GeoB 7101-1 in order to see more productivity proxies.

[20] During the MIS 4–5, accumulation rates of authigenic uranium are low (7 dpm cm^{-2} kyr^{-1}) and during the Holocene/MIS 2 periods, the authigenic U fluxes are high (6–27 dpm cm^{-2} kyr^{-1}) (Figure 6). Unlike opal and organic carbon rain rates, the authigenic U flux do not reveal a cyclicity. Variations of authigenic U fluxes are erratic and do not show any climatic signals. How can we

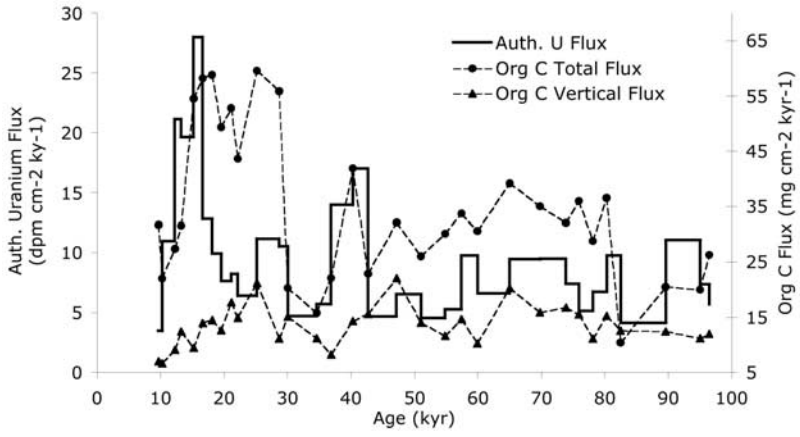

Figure 6. Comparison between authigenic uranium fluxes (dpm cm^{-2} kyr^{-1}) and total and vertical organic carbon fluxes (mg cm^{-2} kyr^{-1}) for the last 100,000 years derived from deep-sea sediment core GeoB 7101-1.

reconcile authigenic U flux with opal and organic carbon? The recent discovery that authigenic U fluxes may also be influenced by lateral transport of organic carbon, or a change of oxygen concentration in water column [*François et al.*, 1997; *Anderson et al.*, 1998; *Frank et al.*, 2000; *Dezileau et al.*, 2002], helps reconcile the authigenic U flux record with those of the other proxies.

[21] The flux of organic carbon to the seabed may be influenced by sediment focusing. That is, focused deposition of sinking particles by deep-sea currents may enhance significantly the local flux of organic matter to the seabed relative to the regional average flux of organic matter exported from surface waters [*Anderson et al.*, 1998; *François et al.*, 1993]. Accumulation of sediments in the continental slope off northern Chile is strongly enhanced by sediment focusing. Lateral transport estimations for the last 100 kyr suggest that sediment redistribution is higher during the LGM and Holocene periods. In that case, we suggest that a significant part of the authigenic U was attributed to intense sediment focusing during these periods (Figure 6).

[22] In the water column, particulate nonlithogenic U (PNU: excess U above detrital background levels) is found in marine particulate matter [*Anderson*, 1982]. *Zheng et al.* [2002] have recently shown that PNU formed in surface waters may, under certain circumstances (i.e., low concentration of oxygen in the water column), contribute significantly to the total burial of authigenic U (between 20% and 80% below the oxygen minimum zone (OMZ) off California). Our two gravity cores were raised below the OMZ, thus, the PNU must certainly contribute significantly to the total burial of authigenic U in this area. Moreover, *Zheng et al.* [2002] showed that the preservation of PNU as particles sink through the water column varies with the water column oxygen content. Evidence for past changes in oxygen concentration in the water column off Peru have been shown by *Ganeshram et al.* [2000]. This means that the oxygen content of the water column off northern Chile have also probably changed between glacial/interglacial periods affecting the contribution of PNU to the total burial of authigenic U. Thus variation in authigenic U in our cores may also be explained by a change in the contribution of PNU due to a change in the water column oxygen concentration. In conclusion, we suggest that the authigenic U flux cannot be used as a direct proxy of palaeoproductivity in the eastern South Pacific.

6. Discussion

6.1. Regional Paleoceanographic and Paleoclimatic Implications

[23] Biogenic opal and organic carbon vertical rain rates and the opal/carbonate ratio (Figures 5a–5c) reveal a strong cyclicity, which is dominated by precession (a cycle of ~20,000 years). High and low values are in phase with summertime (January) insolation maxima and minima, calculated for 25°S latitude from the Earth's known orbital variations [*Berger and Loutre*, 1991]. These variations were in phase during the last 100,000 years. Iron vertical rain rates also show a strong precessional cyclicity. The patterns of iron vertical rain rate and of iron content itself (Figure 5d) are remarkably similar to the down-core records of the proxies for biogenic productivity (Figures 5a–5c), suggesting iron availability to be a factor responsible for past changes in productivity. Although Fe/Al ratios could be affected by the presence of authigenic iron, particularly in low oxygen environments, variations in the La/Yb ratios (Figure 5c), which are not altered by changes in the redox conditions, show the same pattern (see section 5.2). Thus our results indicate that the supply of iron and consequently biological productivity has varied in response to past changes in orbital forcing.

[24] The potential for fertilization of iron-limited waters depends on the source of the iron. Iron supplied in the form of riverine or atmospheric dust is more likely biologically available at the surface than iron from other sources (e.g., lithogenic material transported by deep-ocean currents, for example). Recent studies [*Lamy et al.*, 1998, 2000] on core GeoB 3375-1 have clearly

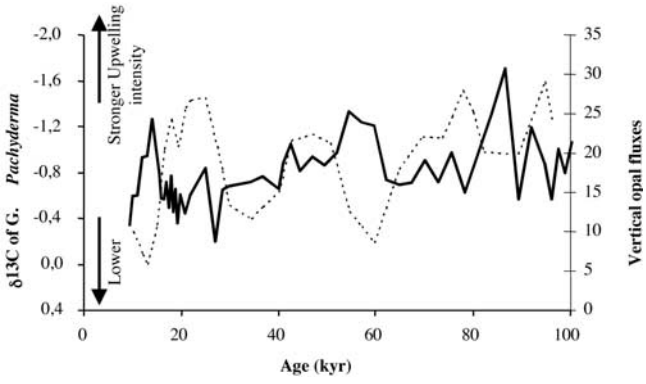

Figure 7. Comparison between the $\delta^{13}C$ of N. *pachyderma* (thick line) and biogenic opal vertical rain rates for the last 100,000 years derived from deep-sea sediment cores GeoB 3375-1 and GeoB 7101-1. The arrows indicate "stronger" or "lower" upwelling intensity using $\delta^{13}C$ of N. *pachyderma* as proxy.

shown that during summer insolation maxima the lithogenic material in this region is mainly of fluvial origin coming from the Andes (Figure 5e), a result that is supported by our data on rare Earth elements (i.e., the La/Yb ratio). We conclude that during these periods, iron fluxes were dominantly of fluvial origin and therefore passed through the surface ocean en route to the seabed. During precessional maxima, biologically available iron associated with this fluvial material should have somewhat relieved iron limitation in this present-day coastal HNLC upwelling regime.

[25] Another hypothesis could be that biological productivity is driven by upwelling. In other words, it was the delivery of large amount of nutrients including iron via upwelling, which stimulated higher biogenic opal and organic carbon vertical rain rates indicative of higher productivity. We here investigate this hypothesis using the $\delta^{13}C$ of N. *pachyderma*. The $\delta^{13}C$ of N. *pachyderma* varies between -0.2 to -1.7‰ (Figure 7). An increase of upwelling intensity would make go up deeper and colder water with lower $\delta^{13}C$ of dissolved inorganic carbon (DIC). Thus, if biological productivity had been only driven by upwelling intensity, we should have observed a correlation between low values of $\delta^{13}C$ of N. *pachyderma* and high opal vertical rain rates (Figure 7). This correlation is not observed. The $\delta^{13}C$ variations are obviously independent of those of the productivity proxies and do not reflect the periodicity recorded for opal fluxes. Moreover, the period of increased productivity observed in our cores do not correlate with the maximal upwelling activity (early MIS 1, MIS 3 and upper MIS 5) in the Peru-Chile current off the Peru margin [*Oberhänsli et al.*, 1990]. In addition, *Schrader and Sorknes* [1990] consider that increased upwelling strength was very slight during these periods. Whatever the upwelling strength was, the Peru Chile current area seemed to have remained a HNLC zone. Within these zones, the physical supply of nutrients exceed the biological demand, consequently an increase of upwelling strength is not needed to increase productivity, a higher utilization of nutrient through iron fertilization would be a more possible explanation. This is illustrated by results obtained by *Lyle et al.* [1992] in the central equatorial Pacific where upwelling strength variations were unable to explain organic carbon burial without taking into account terrestrial input (aeolian) and probably iron fertilization.

[26] We propose that variations in marine productivity at the precessional timescale are due to changes in terrestrial weathering regimes. At present, maximum precipitation in Central Chile [*Aceituno and Vidal*, 1990] is during the austral winter. The increasing amounts of rainfall are directly related to the annual frequency of atmospheric frontal systems arriving from the west, which also increase with latitude (cf. Figure 1). In our study region, the Norte Chico, most of the precipitation is deposited in the form of snow [*Aceituno and Vidal*, 1990] during the winter season. The few rivers here display a clear "snow" regime, with a maximum fluvial runoff during the period of melting (austral summer). During precessional maxima (winter insolation minima), a latitudinal shift toward the north in the patterns of onshore precipitation (cf. Figure 1), for example due to a $\sim 5^{\circ}$ northward displacement of the southern westerlies and thus of the climatic zones in Chile [*Lamy et al.*, 1998], should have occurred. Snow precipitation was probably much higher during the winter and the fluvial runoff more significant during the summer. These periods of higher river runoff should have transported significant amounts of iron-rich terrigenous material from the Andes (high La/Yb and Fe/Al ratio) into the ocean. The high river discharges could then have caused an increase in iron concentrations, as well as an increase in silicate concentrations, in the ocean surface waters and induced an increase in biological productivity in the region, particularly through diatom blooms. During precessional minima, aridity was probably even stronger than today, with low precipitation during the winter and absence of rivers during the summer. Hence the sediment load of the ocean surface waters supplied by river discharges must have been low and iron was not sufficiently available in the ocean surface waters, limiting primary productivity in the region.

[27] An analogous situation in the precipitation and river runoff occurs at the interannual timescale. During El Niño events above average precipitation and river runoff are observed in central Chile [*Aceituno and Vidal*, 1990; *Montecinos and Aceituno*, 2003]; the opposite is observed during La Niña periods. Positive rainfall anomalies during El Niño winters in the region are associated with a northern shift in the storm tracks and enhanced blocking activity over the Amundsen-Bellinghausen Seas [*Montecinos and Aceituno*, 2003]. Hence an El Niño-Southern Oscillation-like mechanism may have modulated the iron supply by rivers at the precessional timescale. An ENSO modeling experiment over the past glacial-interglacial cycles has shown that changes in low-latitude insolation induce variations in the frequency and intensity of ENSO events [*Clement et al.*, 2000]. However, we found that variations in our iron vertical rain rates are not

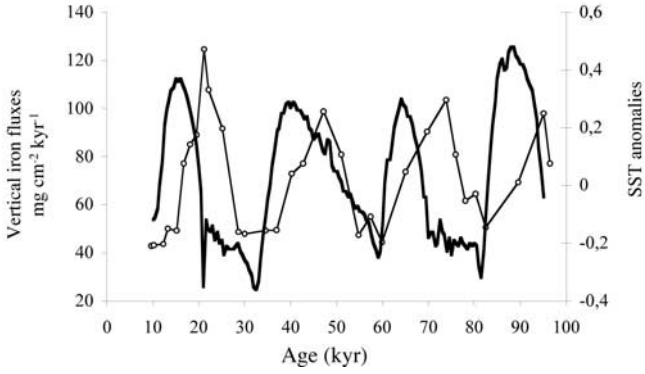

Figure 8. Comparison between iron vertical rain rates (thin line) based on point-by-point normalization to $^{230}Th^{\circ}_{ex}$ and sea surface temperature anomalies (thick line) in the region Niño 3 (5°N–5°S, 150°–90°W) modeled by *Clement et al.* [2000].

in phase with the predictive ENSO model [*Clement et al.*, 2000] at such a timescale (Figure 8), an almost constant shift of about 10 kyr occurs between the model and our iron fluxes. Further studies are thus required to clearly establish the links between rainfall in the region and anomalies in the tropical Pacific at orbital timescales.

6.2. Comparison With Equatorial Upwelling (Peru) During the Last Glacial Maximum

[28] It has been most commonly thought that productivity on the glacial-interglacial timescale in the eastern equatorial Pacific (EEP) was controlled by upwelling and the strength of the tradewinds. The expectation was that stronger winds during glacials would increase the rate of upwelling and raise productivity through increased supply of nutrients.

[29] Several tools have been used to infer past productivity of Peru and Chile Margins. Some were based on accumulation rates of biogenic components (organic carbon, opal and barium accumulation rates) and others based on proxies independent of accumulation rate calculations (abundance of planktic and benthic foraminifera, geochemical proxies). Since there is a risk that the accumulation rates are affected by redistribution of sediment by bottom currents we have decided to take into account only works based on proxies independent of accumulation rate calculations.

[30] Regional reconstruction of productivity patterns by *Loubere* [2000] indicates that in the area downstream of the Peru margin, export productivity was lower during the Last Glacial Maximum (LGM). This interpretation is coincident with results from independent geochemical tracers based on ratios of productivity sensitive elements [*Loubere and Murray*, 2001; *Ganeshram et al.*, 2000]. On the contrary, regional reconstruction of productivity off Chile [study on species composition of planktic foraminifera [*Hebbeln et al.*, 2002; this work] shows that export productivity was higher during the LGM. How can we reconcile the higher productivity off Chile with the lower productivity downstream of the Peru margin?

[31] Presently, nutrients and productivity in the EEP south of the equator reflect the upwelling of deeper Equatorial Undercurrent Water along the margin of Peru. This water has its ultimate source in the SW Pacific subantarctic [*Toggweiler et al.*, 1991], an area where waters are rich in nutrients [*Fitzwater et al.*, 1996]. *Loubere et al.* [2003] proposed that during the LGM the supply of Equatorial Undercurrent Water from the subantarctic was reduced and that there was a proportional increase in water from subtropical sources (poor in nutrients) that upwelled along the Peru margin. The implication of these results is that productivity in the EEP has been strongly affected by ocean circulation rather than just the tradewinds and upwelling alone.

[32] Investigation of surface sediments from the Chilean continental slope points to the Antarctic Circumpolar Current (ACC) as the principal nutrient source that sustains the high productivity in the Humboldt Current, where, besides being slowly consumed, the nutrients are continuously recycled in the coastal upwelling system while moving to the north [*Hebbeln et al.*, 2000]. These nutrients are effectively consumed by marine microorganisms in the coastal upwelling system due to a supplement of iron derived from nearby hinterland and resuspended sediments from the continental shelf. During the LGM, a northward displacement of the ACC (rich in major nutrients, i.e., Si, N and P), in line of the northward movement of the southern westerlies, would bring the main nutrient source closer to our core sites [*Hebbeln et al.*, 2000]. This is, however, not sufficient. With Si (and other major nutrients transported by the ACC) but no Fe being supplied to waters, primary producers in this region would have been probably limited (HNLC conditions). The increase of iron-rich terrigenous material from the Andes during the LGM has permitted an increase of productivity. The implication of this result is that productivity off Chile has also been strongly affected by other processes than just upwelling alone.

[33] In conclusion, productivity in the Chilean upwelling does not vary in the same way than the Peruvian upwelling during the LGM. It seems that two systems work both independently. This result may only be explained by a different origin of nutrients and micronutrients.

6.3. Global Paleoceanographic Implications

[34] Iron limitation of phytoplankton primary productivity in HNLC regions has become a central paradigm in biological oceanography [*Hutchins and Bruland*, 1998; *Martin and Fitzwater*, 1988; *De Baar et al.*, 1990; *Coale et al.*, 1996, 2004; *Hutchins et al.*, 2002] and a main hypothesis [*Martin*, 2000] to explain glacial/interglacial changes in paleoproductivity and atmospheric pCO_2. However, the conventional view has been that variations in productivity in coastal upwelling systems (and their response to orbital forcing) are mainly driven by changes in the meridional surface wind field, and consequently in the input of major nutrients from subsurface to surface waters. Moreover, although fertilization of the photic zone by the upwelling process promotes high primary production and uptake of CO_2 from the atmosphere and the

corresponding high rates of export of carbon to the depth, upwelling promotes also a strong outgassing of CO_2 to the atmosphere. Hence increased upwelling and primary production do not necessarily mean a significant net increase in uptake of atmospheric CO_2. We have shown here that past changes in productivity in the upwelling system of the eastern South Pacific may have been controlled mainly by the availability of Andean iron, through changes in the hydrological conditions, and that this availability has been tightly linked to orbital forcing during the last 100,000 years. Therefore variations in paleoproductivity in major coastal upwelling systems due to iron fertilization may have had a significant influence on past variations in atmospheric pCO_2. However, we also show that the Chilean upwelling region never really has been highly productive in comparison with other upwelling regions or the Southern Ocean in view of the very low biogenic opal deposition and low Corg contents. Thus the potential importance of this region as an area of glacial CO_2 drawdown has most likely been negligible. This is, however, an important result because it has been argued that the middle and low latitude HNLC areas of the oceans such as the coastal upwelling regions may have been an important sink for glacial atmospheric CO_2.

7. Conclusions

[35] We have analyzed variations of ocean productivity through the last 100,000 years in the upwelling system of the eastern South Pacific, as recorded in sediments from two gravity cores retrieved at the same location from the continental slope off northern Chile. We demonstrated that strong changes in accumulation rates recorded in these cores were due to changes in lateral transport by bottom currents rather than reflecting changes in particle settling rates from the overlying water column. In this case, opal and organic carbon accumulation rates cannot be used to assess past changes in productivity. This information can be obtained, however, by normalization to ^{230}Th which corrects for syndepositional sediment redistribution.

[36] Biogenic opal and organic carbon vertical rain rates and the opal/carbonate ratio reveal a strong cyclicity, which is dominated by the precessional period (~20,000 years). Iron vertical rain rates also show a strong precessional cyclicity. The patterns of iron and terrigenous material vertical rain rates are remarkably similar to the down-core records of the proxies for biogenic productivity, suggesting iron availability to be a main factor responsible for past changes in productivity. During precessional maxima increased precipitation in the region, for example due to a northward shift of the southern westerlies or an ENSO-like mechanism, may have brought high inputs of iron from the Andes to the coastal ocean enhancing primary productivity there. During precessional minima, aridity was probably even stronger than today. Hence the sediment load of the ocean surface waters supplied by river discharges must have been low and iron may thus not have been sufficiently available in the ocean surface waters, limiting primary productivity in the region.

Appendix A: Calculating Age-Corrected Excess ^{230}Th Activity at the Time of Deposition

[37] There are two prerequisites for utilization of ^{230}Th data to determine vertical rain rates. First, the measured concentrations of ^{230}Th have to be corrected both for detrital and authigenic contributions produced from decay of ^{234}U in the sediment in order to calculate the amount of ^{230}Th originating from scavenging in the oceanic water column (excess concentrations). Second, an independent timescale for the core is necessary to calculate the corresponding value at the time of deposition, ($^{230}Th^{\circ}_{ex}$), for each measured $^{230}Th_{ex}$ content.

[38] The total ^{238}U measured in the samples consists of two components: uranium present in detrital minerals (^{238}Ud) and authigenic uranium (^{238}U auth) derived from seawater.

[39] Detrital uranium ($^{238}U_d$) is estimated as:

$$^{238}U_d = \left(^{238}U/^{232}Th\right)_d \times {}^{232}Th, \qquad (A1)$$

where $(^{238}U/^{232}Th)_d$ is the detrital U/Th ratio and $(^{232}Th)_s$ is the measured content of ^{232}Th in the sediment samples. ^{232}Th is considered to be exclusively present in detrital minerals [*Anderson*, 1982].

[40] The authigenic uranium (^{238}U auth) contents of the samples were then calculated using the relation:

$$^{238}U_{auth} = {}^{238}U_{meas} - {}^{238}U_d,$$

where $^{238}U_{meas}$ is the measured total uranium content.

[41] In order to calculate the activities of detrital and authigenic uranium, *François et al.* [1993] assumed a $(^{238}U/^{232}Th)_d$ activity ratio of the detrital sediment phase in the range of 0.5 to 1. We use $^{232}Th \times 0.75$, which represents the estimate of the mean activity of detrital ^{238}U in dpm/g [cf. *Wedepohl*, 1995].

[42] The following equations (equation (A1)) are applied to calculate the age-corrected excess ^{230}Th activity (noted $^{230}Th^{\circ}_{ex}$):

$$\begin{aligned} {}^{230}Th_{ex} = {}& {}^{230}Th_{meas.} - \left(^{232}Th \times 0.75\right) \\ & - \left(^{238}U_{auth.} \times \left[\left(1 - e^{-\lambda_{230}\times t}\right)\right.\right. \\ & + \left(\lambda_{230}/\left(\lambda_{230} - \lambda_{234}\right)\right) \times \left(1 - e^{-(\lambda_{230}-\lambda_{234})\times t}\right) \\ & \left.\left. \times \left(\left(^{234}U/^{238}U\right)_i - 1\right)\right]\right) \end{aligned} \qquad (A2)$$

with

$$^{238}U_{auth.} = {}^{238}U_{meas.} - \left(^{232}Th \times 0.75\right),$$

where (^{232}Th × 0.75) represents the estimate of the mean activity of detrital ^{238}U in dpm g^{-1}; λ_{230} and λ_{234} are the corresponding decay constants of the ^{230}Th and ^{234}U; (^{234}U/^{238}U) refers to the initial activity ratio of ^{234}U and ^{238}U at the time of sediment deposition; and t is the age in years estimated from the previously determined stratigraphy. The ^{238}Uauth. term represents the equilibrium activity of ^{230}Th produced from authigenic uranium, assuming uranium precipitation occurred at the time of sediment deposition.

[43] After the stratigraphy is established, the excess activities of ^{230}Th$_{ex}$ are decay-corrected to the time of deposition of the sediment (^{230}Th$^{\circ}_{ex}$):

$$^{230}Th^{\circ}_{ex} = {}^{230}Th_{ex} \times e^{\lambda_{230} t}.$$

Appendix B

[44] There are several assumptions and problems that may lead to uncertainties in calculating the vertical rain rates:

[45] The first assumption is that lateral isopycnal transport of dissolved ^{230}Th within the water column (boundary scavenging) from high to low particle flux areas, is negligible. Boundary scavenging occurs when marginal sediments receive much greater fluxes of particle-reactive elements than open ocean sediments. An increased lateral transport of isotopes along isopycnals should result in increased radionuclide fluxes to the sediment and should coincide with increased sedimentation rates. In this study, core GeoB7101-1 has higher ^{230}Th$_{ex}^{\circ}$ fluxes (Fs) than the ^{230}Th production flux (Fw) (Figure 3b). So, an increased amount of ''boundary scavenging'' due to a higher particle rain rate could explain the high ^{230}Th fluxes. However, several lines of evidence suggest that this effect is unimportant for our core. Indeed, in different oceanic regions, *François et al.* [1990] and *Yu et al.* [2001] showed that while total mass flux collected by sediment traps varied 15-fold between low and high productivity regions, the accompanying flux of ^{230}Th varied from a deficit (compared to ^{230}Th production rate) of circa 40% in oligotrophic regions to an maximum excess of circa 50% in high flux areas. In the extreme case, if we assume a strong upwelling and high mass flux in our study region, the ^{230}Th$_{ex}$ flux may be increased by a factor of 1.5 by boundary scavenging. In that case, only ratios between sediment accumulation rates and vertical sediment rain rates (called focusing factor by *Suman and Bacon* [1989]) above 1.5 may be interpreted as sediment redistribution. For the above reasons, the observed ^{230}Th$^{\circ}_{ex}$ fluxes (Fs) which are up to fivefold the ^{230}Th production flux (Fw) cannot be due to increased boundary scavenging but must have been caused by an increase of the focusing intensity.

[46] The second assumption for estimation of the vertical sediment rain rate is that the ^{230}Th concentration in the redistributed sediment is equal to that of the sediment raining down from the overlying water column (i.e., the redeposited sediment came from an area of similar water depth). As suggested by *François et al.* [1993], it is also possible that the redistributed sediment was initially deposited at a shallower depth prior to being transported to its final site of deposition. In this case, it can be shown that the focusing factor would underestimate the fraction of sediment brought by lateral transport and vertical paleofluxes would overestimate true rain rates. However, several lines of evidence suggest that this problem has not been important for core GeoB7101-1. If lateral transport of sediment initially deposited in shallower areas significantly affected paleoflux estimates, we would expect a correlation between the two, i.e., the higher the focusing factor, the higher the vertical particle rain rate calculated by the ^{230}Th method would be. Since this correlation is not observed (Figures 3a and 3b), the redistributed sediment must have come from an area of similar depth. Moreover, visual examination of the sediment core did not reveal any hints for turbidites throughout the core. Pathways of turbidity currents are channeled and restricted to rare submarine canyons on the continental slope off northern Chile [*Thornburg and Kulm*, 1987].

[47] **Acknowledgments.** We thank A. Montecinos, C. Lange, and T. Platt for useful comments and discussions and R. De Pol and G. Yuras for help with the figures. This work was supported by the Chilean National Commission for Scientific and Technological Research (CONICYT) through the FONDAP Programme. LD was supported by a postdoctoral fellowship from ECOS Sud (France) and Fundación Andes (Chile).

References

Aceituno, P., and F. Vidal (1990), Variabilidad interanual en el caudal de ríos andinos de Chile Central en relación con la temperatura de la superficie del mar en el Pacífico Central, *Rev. Soc. Ing. Hidraul.*, *5*, 9–17.

Anderson, R. F. (1982), Concentration, vertical flux, and remineralization of particulate uranium in seawater, *Geochim. Cosmochim. Acta*, *46*, 1293–1299.

Anderson, R. F., N. Kumar, M. R. A. Mortlock, P. N. Froelich, P. Kubik, B. Dittrich-Hannen, and M. Sutter (1998), Late Quaternary changes in productivity of the Southern Ocean, *J. Mar. Syst.*, *17*, 497–514.

Anderson, R. F., Z. Chase, M. Q. Fleisher, and J. Sachs (2002), The Southern Ocean's biological pump during the Last Glacial Maximum, *Deep Sea Res. Part II*, *49*, 1909–1938.

Arrhenius, G. (1952), Sediment cores from the east Pacific, *Deep Sea Exped.*, *5*, 189–201.

Bacon, M. P. (1984), Glacial to interglacial changes in carbonate and clay sedimentation in the Atlantic ocean estimated from ^{230}Th measurements, *Isot. Geosci.*, *2*, 97–111.

Bentaleb, I., C. Caratini, M. Fontugne, M. T. Morzadec-Kerfourn, J. P. Pascal, and C. Tissot (1997), Monsoon regime variations during the late Holocene in the southwestern India, in *Third Millennium BC Social Collapse and Climate Change*, edited by N. Dalfes, G. Kukla, and H. Weiss, pp. 475–488, Springer-Verlag, New York.

Berger, A., and P. J. Loutre (1991), Insolation values for the climate of the last 10 million years, *Quat. Sci. Rev.*, *10*, 297–317.

Berger, W. H., V. S. Smetacek, and G. Wefer (1989), Ocean productivity and paleoproduc-

tivity—An overview, in *Productivity of the Ocean: Present and Past*, edited by W. H. Berger, V. S. Smetacek, and G. Wefer, pp. 1–34, John Wiley, Hoboken, N. J.

Brink, K. H., and T. J. Cowles (1991), The coastal transition zone program, *J. Geophys. Res.*, *96*, 14,637–14,648.

Broecker, W. S. (1982), Glacial to interglacial changes in ocean chemistry, *Prog. Oceanogr.*, *11*, 151–197.

Chase, Z., R. F. A. Anderson, M. Q. F. Fleisher, and P. W. Kubik (2003), Accumulation of biogenic and lithogenic material in the Pacific sector of the Southern Ocean during the past 40,000 years, *Deep Sea Res. Part II*, *50*, 799–832.

Clement, A. C., R. Seager, and M. A. Cane (2000), Suppression of El Niño during the mid-Holocene by changes in the Earth's orbit, *Paleoceanography*, *15*, 731–737.

Coale, K. H., et al. (1996), A massive phytoplankton bloom induced by an ecosystem-scale iron fertilization experiment in the equatorial Pacific Ocean, *Nature*, *383*, 495–501.

Coale, K. H., et al. (2004), Southern Ocean iron enrichment experiment: Carbon cycling in High and low Si waters, *Science*, *304*, 408–414.

Daneri, G., et al. (2000), Primary production and community respiration in the Humboldt Current system off Chile and associated oceanic areas, *Mar. Ecol. Prog. Ser.*, *197*, 41–49.

De Baar, H. J. W., et al. (1990), On iron limitation of the Southern Ocean: Experimental observations in the Weddell and Scotia Seas, *Mar. Ecol. Prog. Ser.*, *65*, 105–122.

Dezileau, L., G. Bareille, J. L. Reyss, and F. Lemoine (2000), Evidence for strong sediment redistribution by bottom currents along the Southeast Indian Ridge, *Deep Sea Res. Part I*, *47*, 1899–1936.

Dezileau, L., G. Bareille, and J. L. Reyss (2002), Enrichments in authigenic uranium in glacial sediments of the Southern Ocean, *C. R. Geosci.*, *334*, 1039–1046.

Dezileau, L., J. L. Reyss, and F. Lemoine (2003), Late Quaternary changes in biogenic opal fluxes in the Southern Indian Ocean, *Mar. Geol.*, *202*, 143–158.

Emerson, S., and J. I. Hedges (1988), Processes controlling the organic carbon content of open ocean sediments, *Paleoceanography*, *3*, 621–634.

Fitzwater, S. E., K. H. Coale, R. M. Gordon, K. S. Johnson, and M. E. Ondrusek (1996), Iron deficiency and phytoplankton growth in the equatorial Pacific, *Deep Sea Res. Part II*, *43*, 995–1015.

Fontugne, M. R., and J. C. Duplessy (1981), Organic carbon isotopes fractionation by marine plankton in the temperate range −1 to 31°C, *Oceanol. Acta*, *4*, 85–90.

François, R., M. P. Bacon, and D. O. Suman (1990), Thorium 230 profiling in deep-sea sediments: High-resolution records of flux and dissolution of carbonate in the equatorial Atlantic during the last 24,000 years, *Paleoceanography*, *5*(5), 761–787.

François, R., M. P. Bacon, M. A. Altabet, and L. D. Labeyrie (1993), Glacial/interglacial changes in sediment rain rate in the SW Indian sector of Subantarctic waters as recorded by ^{230}Th, ^{231}Pa, U, and δ^{15}N, *Paleoceanography*, *8*(5), 611–629.

François, R., M. A. Altabet, E.-F. Yu, D. M. Sigman, M. Frank, M. P. Bacon, G. Bohrmann, G. Bareille, and L. D. Labeyrie (1997), Contribution of southern ocean surface-water stratification to low atmospheric CO_2 concentrations during the last glacial period, *Nature*, *389*, 929–935.

François, R., M. Frank, M. M. Rutgers van der Loeff, and M. P. Bacon (2004), ^{230}Th normalization: An essential tool for interpreting sedimentary fluxes during the late Quaternary, *Paleoceanography*, *19*, PA1018, doi:10.1029/2003PA000939.

Frank, M., A. Eisenhauer, W. J. Bonn, P. Walter, H. Grobe, P. W. Kubik, B. Dittrich-Hannen, and A. Mangini (1995), Sediment redistribution versus paleproductivity change: Weddell Sea margin sediment stratigraphy and biogenic particle flux of the last 250.000 years deduced from ^{230}Thex, ^{10}Be and biogenic barium profiles, *Earth Planet. Sci. Lett.*, *136*, 559–573.

Frank, M., R. Gersonde, M. Rutgers Van der Loeff, G. Bohrmann, C. C. Nurnberg, P. W. Kubik, M. Suter, and A. Mangini (2000), Similar glacial and interglacial export bioproductivity in the Atlantic sector of the Southern Ocean: Multiproxy evidence and implications for glacial atmospheric CO_2, *Paleoceanography*, *15*(6), 642–658.

Ganeshram, R., T. Pedersen, S. Calvert, G. McNeill, and M. Fontugne (2000), Glacial-interglacial variability in denitrification in the world's ocean: Causes and consequences, *Paleoceanography*, *15*, 361–376.

Hebbeln, D., M. Marchant, T. Freudenthal, and G. Wefer (2000), Surface sediment distribution along the Chilean continental slope related to upwelling and productivity, *Mar. Geol.*, *164*, 119–137.

Hebbeln, D., M. Marchant, and G. Wefer (2002), Paleoproductivity in the southern Peru-Chile Current through the last 33,000 years, *Mar. Geol.*, *186*, 487–504.

Henderson, G. M., C. Heinze, R. F. Anderson, and A. M. E. Winguth (1999), Global distribution of the ^{230}Th flux to ocean sediments constrained by GCM modelling, *Deep Sea Res. Part*, *46*, 1861–1893.

Hutchins, D. A., and K. W. Bruland (1998), Iron-limited diatom growth and Si:N uptake ratios in a coastal upwelling regime, *Nature*, *393*, 561–564.

Hutchins, D. A., et al. (2002), Phytoplankton iron limitation in the Humboldt Current and Peru upwelling, *Limnol. Oceanogr.*, *47*, 997–1011.

Kay, S. M., C. Mpodozis, V. A. Ramos, and F. Munizaga (1991), Magma source variations for mid-late Tertiary magmatic rock associated with a shallowing subduction zone and a thickening crust in the central Andes (28–33 S), in *Andean Magmatism and Its Tectonic Setting*, *Spec. Pap.*, vol. 265, edited by R. S. Harmon and C. W. Rapela, pp. 113–137, Geol. Soc. of Am., Boulder, Colo.

Kumar, N., R. F. Anderson, R. A. Mortlock, P. N. Froelich, P. Kubik, P. Dittrich-Hannen, and M. Suter (1995), Increased biological productivity and export production in glacial Southern Ocean, *Nature*, *378*, 675–680.

Lamy, F., D. Hebbeln, and G. Wefer (1998), Late Quaternary precessional cycles of terrigenous sediment input off the Norte Chico, Chile (27.5°S) and paleoclimatic implications, *Palaeogeogr. Palaeoclimatol. Palaeoecol.*, *141*, 233–251.

Lamy, F., J. Klump, D. Hebbeln, and G. Wefer (2000), Late Quaternary rapid climate change in northern Chile, *Terra Nova*, *12*, 8–13.

Longhurst, A., S. Sathyendranath, T. Platt, and C. Caverhill (1995), An estimate of global primary production in the ocean from satellite radiometer data, *J. Plankton Res.*, *17*, 1245–1271.

Loubere, P. (2000), Marine control of biological production in the eastern equatorial Pacific Ocean, *Nature*, *406*, 497–500.

Loubere, P., and R. Murray (2001), Late Pleistocene bioproductivity in the eastern equatorial Pacific: Patterns and comparison of proxies, *Eos Trans. AGU*, *82*(20), Abstract PP12A-0478.

Loubere, P., M. Fariduddin, and R. W. Murray (2003), Patterns of export production in the eastern equatorial Pacific over the past 130,000 years, *Paleoceanography*, *18*(2), 1028, doi:10.1029/2001PA000658.

Lyle, M., D. W. Murray, B. P. Finney, J. Dymond, J. M. Robbins, and K. Brooksforce (1988), The record of late Pleistocene biogenic sedimentation in the eastern tropical Pacific Ocean, *Paleoceanography*, *3*, 39–59.

Lyle, M. W., F. G. Prahl, and M. A. Sparrow (1992), Upwelling and productivity changes inferred from a temperature record in the central equatorial Pacific, *Nature*, *355*, 812–815.

Mariotti, A., F. Gadel, P. Giresse, and X. Kinga-Mouzeo (1991), Carbon isotope compositions and geochemistry of particulate organic matter in the Congo river: Application to the study of quaternary sediments of the mouth river, *Chem. Geol.*, *86*, 345–357.

Martin, J. H. (2000), Glacial-interglacial CO_2 change: The iron hypothesis, *Paleoceanography*, *5*, 1–13.

Martin, J. H., and S. E. Fitzwater (1988), Iron deficiency limits phytoplankton growth in the northeast Pacific subarctic, *Nature*, *331*, 341–343.

Montecinos, A., and P. Aceituno (2003), Seasonality of the ENSO-related rainfall variability in central Chile and associated circulation anomalies, *J. Clim.*, *16*, 281–296.

Müller, P. J., and R. Schneider (1993), An automated leaching method for the determination of opal in sediments and particulate matter, *Deep Sea Res.*, *40*, 425–444.

Oberhänsli, H., P. Heinze, L. Diester-Haass, and G. Wefer (1990), Upwelling off Peru during the last 430,000 yr and its relationship to the bottom water environment, as deduced from coarse grain size distributions and analyses of benthic foraminifers at hole 679D and 681B, Leg 112, *Proc. Ocean Drill. Project, Sci. Results*, *112*, 369–390.

Paillard, D., L. Labeyrie, and P. Yiou (1996), Macintosh program performs time-series analysis, *Eos Trans. AGU*, *77*, 379.

Pedersen, T. F., and S. E. Calvert (1990), Anoxia versus productivity: What controls the formation of organic carbon rich sediments and sedimentary rocks?, *AAPG Bull.*, *74*, 454–466.

Pichowiak, S. (1994), Early Jurassic to early Cretaceous magmatism in the coastal cordillera and the central depression of north Chile, in *Tectonics of the Southern Central Andes*, edited by Reutter, Scheuber, and Wigger, pp. 203–217, Springer-Verlag, New York.

Quay, P. D., D. O. Wilbur, J. E. Richey, J. I. Hedges, A. H. Devol, and R. Victoria (1992), Carbon cycling in the Amazon River: Implication from the 13C compositions of particles and solutes, *Limnol. Oceanogr.*, *37*, 857–871.

Sarnthein, M., K. Winn, J. C. Duplessy, and M. R. Fontugne (1988), Global variations of surface ocean productivity in low and mid latitudes: Influence on CO_2 reservoirs of the

deep ocean and atmosphere during the last 21,000 years, *Paleoceanography*, *3*, 361–399.
Schneider, E. K., Z. Zhu, B. S. Giese, B. Huang, B. P. Kirtman, J. Shukla, and J. A. Carton (1997), Annual cycle and ENSO in a coupled ocean-atmosphere general circulation model, *Mon. Weather Rev.*, *125*, 680–702.
Schrader, H., and R. Sorknes (1990), Spatial and temporal variation of Peruvian coastal upwelling during the latest Quaternary, Leg 112, *Proc. Ocean Drill. Project, Sci. Results*, *112*, 391–406.
Suman, D. O., and M. P. Bacon (1989), Variations in Holocene sedimentation in the North American basin determined from ^{230}Th measurements, *Deep Sea Res.*, *36*(6), 869–878.
Summerhayes, C. P., K.-C. Emeis, M. V. Angel, R. L. Smith, and B. Zeitzschel (1995), Upwelling in the ocean: Modern processes and ancient records, in *Upwelling in the Ocean: Modern Processes and Ancient Records*, edited by C. P. Summerhayes pp. 1–37, John Wiley, Hoboken, N. J.
Thornburg, T. M., and L. D. Kulm (1987), Sedimentation in the Chile Trench: Depositional morphologies, lithofacies, and stratigraphy, *Geol. Soc. Am. Bull.*, *98*, 33–52.
Toggweiler, J., D. Dixon, and W. Broecker (1991), The Peru upwelling and the ventilation of the South Pacific thermocline, *J. Geophys. Res.*, *96*, 20,467–20,497.
Wedepohl, K. H. (1995), The composition of the continental crust, *Geochim. Cosmochim. Acta*, *59*, 1217–1232.
Yu, E. F., R. Francois, M. P. Bacon, and A. P. Fleer (2001), Fluxes of ^{230}Th and ^{231}Pa to the deep sea: Implications for the interpretation of excess ^{230}Th and ^{231}Pa/^{230}Th profiles in sediments, *Earth. Planet. Sci. Lett.*, *191*, 219–230.
Zheng, Y., R. F. Anderson, A. Van Geen, and M. Q. Fleisher (2002), Preservation of particulate non-lithogenic uranium in marine sediments, *Geochim. Cosmochim. Acta*, *66*(17), 3085–3092.

L. Dezileau, Laboratoire de Dynamique de la Lithosphère, Université de Montpellier 2, Montpellier F-34095, France. (dezileau@dstu.univ-montp2.fr)

M. Fontugne and J.-L. Reyss, Laboratoire des Sciences du Climat et de l'Environnement, CNRS/Commissariat à l'Energie Atomique, F-91198 Gif-sur-Yvette, France.

D. Hebbeln and F. Lamy, Fachbereich Geowissenschaften, Universität Bremen, Postfach 330440, D-28334 Bremen, Germany.

O. Ulloa, Centro de Investigación Oceanográfica, Programa Regional de Oceanografía Fisica y Clima, Departamento de Oceanografía, Universidad de Concepción, Concepción, Chile.

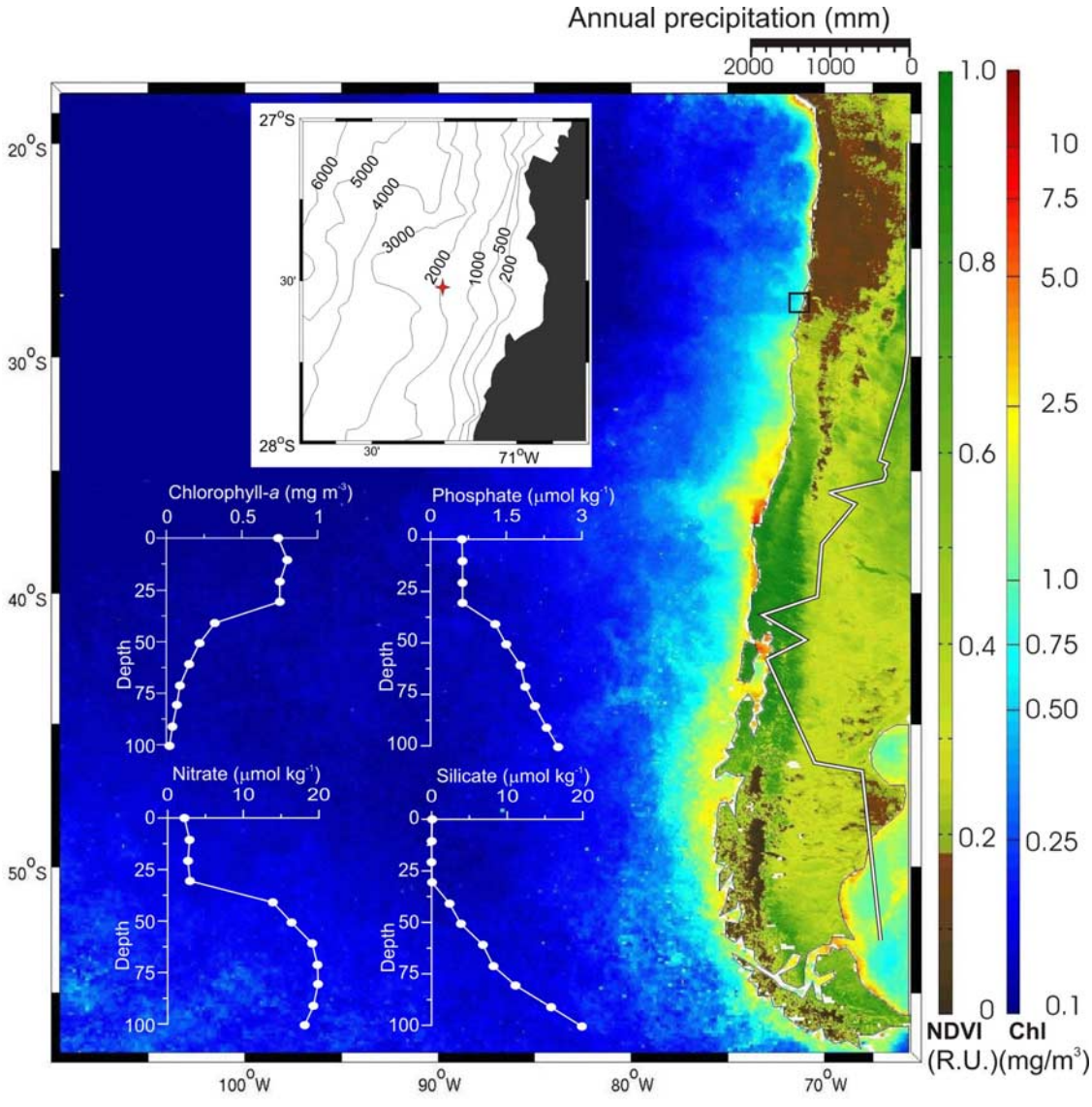

Figure 1. Composite of annual average of phytoplankton pigment concentration (Chl) of the eastern South Pacific and annual maximum normalized difference vegetation index (NDVI) of the central and southern Andean region (both for year 2000). These data were derived from the SeaWiFS sensor (SeaWiFS Project) Distributed Active Archive Center. Top left inset: map of the study area with location of the two cores GeoB 3375-1 and GeoB 7101-1 (27°28′S, 71°15′W). Bottom left inset: chlorophyll and nutrient profiles of the upper 100 m depth at station GeoB 3377-1 (27°28′S; 71°31.5′W). Right inset: average of annual continental rainfall data in Chile (http://www.meteochile.cl).